Acta Crystallographica Section D
Biological Crystallography
ISSN 0907-4449

Structures of *Burkholderia thailandensis* nucleoside kinase: implications for the catalytic mechanism and nucleoside selectivity

Yoshiaki Yasutake,[a]‡ Hiroko Ota,[b]‡ Emisa Hino,[b] Shin-ichi Sakasegawa[b] and Tomohiro Tamura[a,c]*

[a]Bioproduction Research Institute, National Institute of Advanced Industrial Science and Technology (AIST), 2-17-2-1 Tsukisamu-Higashi, Toyohira-ku, Sapporo 062-8517, Japan, [b]Asahi Kasei Pharma Corporation, 632-1 Izunokuni, Shizuoka 410-2321, Japan, and [c]Laboratory of Molecular Environmental Microbiology, Graduate School of Agriculture, Hokkaido University, Kita-9, Nishi-9, Kita-ku, Sapporo 060-8589, Japan

‡ These authors contributed equally to this work.

Correspondence e-mail: t-tamura@aist.go.jp

Received 1 August 2011
Accepted 21 September 2011

PDB References: BthNK, 3b1o; BthNK–ADP–MZR, 3b1n; BthNK–ADP–INO, 3b1p; BthNK–INO, 3b1q; BthNK–AMP–Mg^{2+}–AMP, 3b1r.

The nucleoside kinase (NK) from the mesophilic Gram-negative bacterium *Burkholderia thailandensis* (BthNK) is a member of the phosphofructokinase B (Pfk-B) family and catalyzes the Mg^{2+}- and ATP-dependent phosphorylation of a broad range of nucleosides such as inosine (INO), adenosine (ADO) and mizoribine (MZR). BthNK is currently used in clinical practice to measure serum MZR levels. Here, crystal structures of BthNK in a ligand-free form and in complexes with INO, INO–ADP, MZR–ADP and AMP–Mg^{2+}–AMP are described. The typical homodimeric architecture of Pfk-B enzymes was detected in three distinct conformational states: an asymmetric dimer with one subunit in an open conformation and the other in a closed conformation (the ligand-free form), a closed conformation (the binary complex with INO) and a fully closed conformation (the other ternary and quaternary complexes). The previously unreported fully closed structures suggest the possibility that Mg^{2+} might directly interact with the β- and γ-phosphates of ATP to maintain neutralization of the negative charge throughout the reaction. The nucleoside-complex structures also showed that the base moiety of the bound nucleoside is partly exposed to the solvent, thereby enabling the recognition of a wide range of nucleoside bases. Gly170 is responsible for the solvent accessibility of the base moiety and is assumed to be a key residue for the broad nucleoside recognition of BthNK. Remarkably, the G170Q mutation increases the specificity of BthNK for ADO. These findings provide insight into the conformational dynamics, catalytic mechanism and nucleoside selectivity of BthNK and related enzymes.

1. Introduction

Mizoribine (MZR; 5-hydroxy-1-β-D-ribofuranosyl-1*H*-imidazole-4-carboxamide) is a purine-nucleoside analogue isolated from *Eupenicillium brefeldianum* M-2166 (Mizuno *et al.*, 1974). MZR is currently used as an immunosuppressant after renal transplantation, for lupus nephritis, rheumatoid arthritis and primary nephritic syndrome (Abe *et al.*, 2004). MZR is rapidly absorbed and phosphorylated to mizoribine 5′-monophosphate (MZR-P) intracellularly by adenosine (ADO) kinase. MZR-P acts as a competitive inhibitor of inosine 5′-monophosphate dehydrogenase (IMPDH) and guanosine monophosphate synthetase, which are crucial for *de novo* nucleic

© 2011 International Union of Crystallography
Printed in Singapore – all rights reserved

acid biosynthesis (Koyama & Tsuji, 1983; Kusumi *et al.*, 1989). Because proliferation of T and B cells highly depends on the *de novo* DNA-synthesis pathway, MZR-P exhibits immunosuppressive activity (Yokota, 2002). However, MZR dosage should be determined by measuring serum MZR levels in order to avoid negative effects (Stypinski *et al.*, 2007). We have previously developed a novel method for measuring serum MZR levels that consists of two independent enzymatic reactions catalyzed by two thermostable and soluble bacterial enzymes: (i) the phosphorylation of MZR to MZR-P by Bth_I1158 from *Burkholderia thailandensis* and (ii) the inhibition of *Bacillus subtilis* IMPDH activity by MZR-P (Ota, Yasuda *et al.*, 2008; Hiramitsu *et al.*, 2011).

Bth_I1158 (UniProt database code Q2SZE4) belongs to the phosphofructokinase B (Pfk-B) family (Pfam PF00294; Wu *et al.*, 1991) and has been annotated as a putative ribokinase. However, our previous work revealed that it phosphorylates MZR by using ATP as a phosphoryl donor (Ota, Sakasegawa *et al.*, 2008). Among the various bacterial ribokinase and ADO kinase homologues tested, Bth_I1158 is the only enzyme that effectively converts MZR to MZR-P (unpublished results). Bth_I1158 shows an unusual substrate promiscuity that includes purine nucleosides, purine-analogue nucleosides and uridine, while it shows no activity towards sugars and sugar-phosphates such as D-ribose, fructose, glucose, ribose 5-phosphate and fructose 6-phosphate. Bth_I1158 is therefore considered to be a ribonucleoside kinase (BthNK) rather than a ribokinase. Inosine (INO) and adenosine (ADO) are good substrates for BthNK, and thus BthNK is probably involved in the metabolism of these nucleosides in *B. thailandensis* cells. A sequence-similarity search of the Protein Data Bank (PDB) shows that crystal structures of several BthNK homologues have been reported. The ADO kinase from *Mycobacterium tuberculosis* (MtADK) shows the highest homology to BthNK, with a sequence identity of 36% (Long *et al.*, 2003; Reddy *et al.*, 2007). Interestingly, MtADK is highly specific for ADO and ADO analogues (Long *et al.*, 2003), despite possessing the same active-site residues as BthNK. MtADK is one of the prodrug targets for antitubercular treatment, and some ADO analogues such as 2-methyladenosine act as pro-inhibitors in *M. tuberculosis*. The NK from the hyperthermophilic archaeon *Methanocaldococcus jannaschii* (MjNK) has broad substrate specificity similar to BthNK, but its sequence identity is only 28% (Hansen *et al.*, 2007). Although the structure of MjNK has been reported in complex with ADO and ATP analogues (Arnfors *et al.*, 2006), structural information on its interaction with other nucleosides is not available. Sequence alignment suggests that several amino-acid residues that are essential for substrate binding in BthNK are not conserved in MjNK. Although these nucleoside kinases are evolutionarily closely related to each other in the highly diversified Pfk family (Cabrera *et al.*, 2010), the structural mechanism of nucleoside selectivity remains unclear. In the present study, the X-ray structures of ligand-free BthNK and of BthNK in complex with INO, INO–ADP, MZR–ADP and AMP–Mg^{2+}–AMP were solved at 1.55–2.1 Å resolution. Three distinct conformational states of the BthNK monomer were observed, namely open, closed and fully closed conformations. Moreover, the ligand-complex structures and their comparison with those of related homologues provide insights into the catalytic mechanism and nucleoside selectivity of the kinase.

2. Materials and methods

2.1. Materials

Escherichia coli XL1-Blue cells (Stratagene, La Jolla, California, USA) were used for routine plasmid preparation. The plasmid DNA purification kit was purchased from Promega (Madison, Wisconsin, USA). All restriction enzymes were purchased from New England Biolabs (Beverly, Massachusetts, USA). The DNA ligation kit was purchased from Takara (Otsu, Japan). MZR was provided by Asahi Kasei Pharma Co. Ltd (Shizuoka, Japan). All other chemicals were purchased from Sigma (St Louis, Missouri, USA) and Wako Pure Chemicals (Osaka, Japan). The crystallization screening kits were purchased from Hampton Research (Aliso Viejo, California, USA) and Emerald BioSystems (Bainbridge Island, Washington, USA). The pTip expression vector using *Rhodococcus erythropolis* was developed in our laboratory (Mitani *et al.*, 2005; Nakashima & Tamura, 2004).

2.2. Recombinant protein expression and purification

The expression of BthNK in *E. coli* inhibited cell growth, probably owing to the harmful influence of BthNK on the nucleotide metabolism of *E. coli*. Thus, *R. erythropolis* was used as a heterologous expression host (Ota, Sakasegawa *et al.*, 2008). The gene encoding BthNK was cloned and inserted into a pTip-QC2 expression plasmid and recombinant proteins containing a His_6 tag at either the N-terminus or the C-terminus were overexpressed in *R. erythropolis* L88 cells. The G170Q mutant was prepared using inverse PCR (Hemsley *et al.*, 1989) with the appropriate synthetic oligonucleotides as primers and pTip-QC2-BthNK as the template. Overexpression was induced by the addition of 1 µg ml^{-1} thiostrepton for 24 h at 301 K in Luria–Bertani (LB) medium. The cells were harvested and resuspended in a buffer consisting of 50 m*M* sodium phosphate pH 7.5, 300 m*M* NaCl. The cells were lysed by sonication and the homogenate was clarified by centrifugation. The supernatant was applied onto an Ni-affinity column (His-Select; Sigma) and the column was washed with three column volumes of buffer *A* (50 m*M* sodium phosphate pH 6.0, 300 m*M* NaCl). The His-tagged BthNK was eluted with a linear gradient of 0–400 m*M* imidazole in buffer *A*. The peak fractions containing BthNK were collected and dialyzed against a buffer consisting of 20 m*M* Tris pH 9.0, 50 m*M* NaCl and 2 m*M* DTT. The sample was concentrated to 8 mg ml^{-1} using a centrifugal ultrafiltration device with a 30 kDa cutoff membrane (Milipore, Billerica, Massachusetts, USA).

2.3. Crystallization and X-ray diffraction studies

All crystallization trials were performed at 293 K using either the sitting-drop or the hanging-drop vapour-diffusion

Table 1
X-ray diffraction, SAD phasing and model refinement statistics.

Values in parentheses are for the highest resolution shell.

	MZR–ADP	Ligand-free	MZR–ADP	INO–ADP	INO	AMP–Mg^{2+}–AMP†
PDB code	—	3b1o	3b1n	3b1p	3b1q	3b1r
No. of subunits in asymmetric unit	2	2	2	1	6	6
Subunit conformations	Fully closed	Closed/open	Fully closed	Fully closed	Closed	Fully closed
Data collection	Br-SAD	Native				
Beamline	PF-BL5A	AR-NW12A	AR-NE3A	AR-NE3A	AR-NE3A	AR-NW12A
Wavelength (Å)	0.91957	1.0000	1.0000	1.0000	1.0000	1.0000
Space group	$C222_1$	$P4_12_12$	$C222_1$	$P2_12_12$	$P1$	$P3_1$
Unit-cell parameters (Å, °)						
a (Å)	44.6	85.4	44.6	74.9	83.1	125.2
b (Å)	164.9	85.4	164.7	83.8	85.9	125.2
c (Å)	181.1	160.8	182.5	52.9	86.9	115.0
α (°)	90	90	90	90	66.3	90
β (°)	90	90	90	90	68.5	90
γ (°)	90	90	90	90	67.8	120
V_M (Å^3 Da^{-1})	2.3	2.1	2.3	2.3	2.4	2.5
Solvent content (%)	47.5	40.0	47.5	47.0	48.1	50.3
Resolution range (Å)	50–2.20 (2.32–2.20)	50–2.10 (2.21–2.10)	50–1.55 (1.58–1.55)	50–1.70 (1.73–1.70)	50–1.70 (1.73–1.70)	50–2.00 (2.11–2.00)
Unique reflections	34613	35578	97659	37278	208756	136213
Multiplicity	7.0 (6.8)	12.0 (9.6)	7.0 (6.8)	7.1 (6.1)	3.9 (3.6)	5.6 (5.3)
Completeness (%)	99.9 (99.9)	100.0 (100.0)	99.9 (100.0)	99.4 (92.6)	97.2 (94.0)	99.0 (100.0)
$\langle I/\sigma(I)\rangle$	13.9 (5.6)	11.4 (8.3)	25.9 (5.9)	27.4 (5.3)	19.1 (2.8)	14.7 (4.3)
R_{merge}‡	0.112 (0.359)	0.097 (0.413)	0.072 (0.438)	0.077 (0.281)	0.056 (0.376)	0.083 (0.419)
SAD phasing						
No. of Br sites	28					
FOM§	0.26					
FOM (after *RESOLVE*)§	0.71					
Model refinement						
R_{work}¶		0.236	0.167	0.182	0.176	0.167
R_{free}¶		0.277	0.198	0.217	0.207	0.204
R.m.s.d. bond lengths (Å)		0.009	0.018	0.020	0.019	0.010
R.m.s.d. bond angles (°)		1.22	1.90	1.87	1.84	1.39
Total No. of atoms		4900	5742	2783	15316	15572
Average B factors (Å^2)						
Overall		36.9	17.7	21.0	24.6	22.9
Ligand (nucleoside-binding site)		—	12.8 [MZR]	14.7 [INO]	15.9 [INO]	15.8 [AMP–Mg^{2+}]
Ligand (ATP-binding site)		—	10.6 [ADP]	14.1 [ADP]	—	19.1 [AMP]
Ramachandran plot						
Favoured (%)		89.8	92.1	93.3	92.2	91.1
Allowed (%)		10.2	7.9	6.7	7.8	8.9
Outliers (%)		0.0	0.0	0.0	0.0	0.0

† The model was refined with the twinning operator $(-h, h+k, -l)$. ‡ $R_{merge} = \sum_{hkl}\sum_i |I_i(hkl) - \langle I(hkl)\rangle| / \sum_{hkl}\sum_i I_i(hkl)$, where $\langle I(hkl)\rangle$ is the mean intensity of a set of equivalent reflections. § FOM is the mean figure of merit. ¶ $R_{work} = \sum_{hkl} ||F_{obs}| - |F_{calc}|| / \sum_{hkl} |F_{obs}|$ for the 95% of the reflection data used in the refinement. F_{obs} and F_{calc} are observed and calculated structure-factor amplitudes, respectively. R_{free} is the equivalent of R_{work}, except that it was calculated for a randomly chosen 5% test set that was excluded from refinement.

technique. The protein stock solution was mixed with an equal volume of precipitant solution (1–2 µl) and equilibrated against a reservoir containing the same precipitant solution (100–500 µl). Initial trials were carried out in 96-well sitting-drop plates using sparse-matrix screens. Further optimization of hit conditions was performed in 24-well plates. The ligand-free BthNK was crystallized using 0.1 *M* CHES pH 9.3, 0.2 *M* NaCl, 1.4 *M* ammonium sulfate. For crystallization of the various ligand complexes, protein stock solution (8 mg ml^{-1}) was pre-incubated overnight at 277 K with ligands (2 m*M* ADP, 4 m*M* INO or 30 m*M* MZR). The BthNK–INO binary complex was crystallized using 0.1 *M* sodium acetate pH 4.0, 0.2 *M* calcium acetate, 26% PEG 400. Crystals of the AMP–Mg^{2+}–AMP quaternary complex were obtained using 0.1 *M* Tris pH 7.0, 0.2 *M* $MgCl_2$, 10% PEG 8000. BthNK–INO–ADP and BthNK–MZR–ADP ternary-complex crystals were grown using 0.1 *M* sodium citrate pH 5.1–5.5, 12–16% PEG 3350. X-ray diffraction experiments (Table 1) were carried out at the Photon Factory (Tsukuba, Japan) using a charge-coupled device (CCD) detector (ADSC). Prior to data-collection experiments, the crystals were cryoprotected using 20% glycerol or Paratone-N (Hampton Research) and flash-cooled in a liquid-nitrogen gas stream at 100 K. The diffraction data were processed using either *HKL*-2000 (Otwinowski & Minor, 1997) or *iMOSFLM*/*SCALA* (Battye *et al.*, 2011; Winn *et al.*, 2011).

2.4. Structure solution and model refinement

The structure of BthNK was solved by bromide single-wavelength anomalous diffraction (SAD) phasing (Dauter *et al.*, 2000). A crystal of BthNK in the $C222_1$ form (BthNK–MZR–ADP ternary complex) was soaked stepwise in a cryoprotectant solution supplemented with 0.5 *M* and then 1.0 *M* NaBr with an overall soaking time of approximately 30 s. A 2.2 Å resolution SAD data set was collected at a wavelength

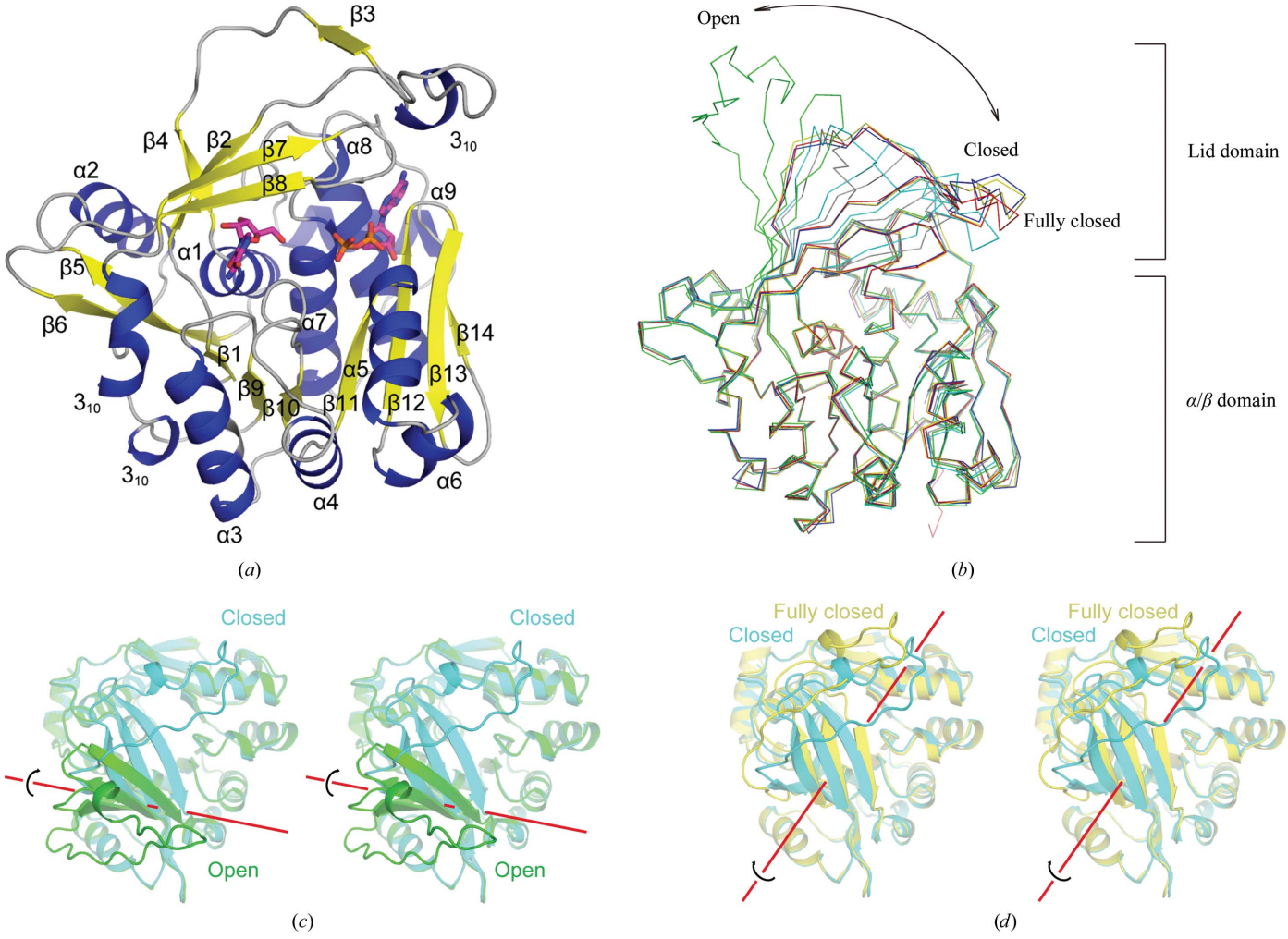

Figure 1
Subunit structure of BthNK. (*a*) Subunit structure of BthNK in complex with MZR–ADP (fully closed form). Secondary-structure elements were assigned using the program *STRIDE* (Heinig & Frishman, 2004). (*b*) Superimposition of subunit structures in the open (chain *B* of the ligand-free structure, green), closed (chain *A* of the INO complex, cyan) and fully closed conformations (INO–ADP complex, blue; chain *A* of the MZR–ADP complex, red; chain *A* of the AMP–Mg^{2+}–AMP complex, yellow) in the same orientation as in (*a*). The structure superimposition was performed using only α/β domains. (*c*) Stereo drawing depicting the domain motion between the open (chain *B* of the ligand-free structure, green) and closed conformations (chain *A* of the ligand-free structure, cyan). (*d*) Stereo drawing depicting the domain motion between the closed (chain *A* of the ligand-free structure, cyan) and fully closed conformations (chain *A* of the AMP–Mg^{2+}–AMP complex, yellow) in the same orientation as in (*c*). The interdomain rotation axes analyzed by *DynDom* (Hayward & Berendsen, 1998) are also shown in red.

of 0.91989 Å where, from a fluorescence scan of the Br *K* absorption edge, f'' for the bromide was estimated to be maximal. A total of 28 bromide binding sites were determined using the program *SHELX* (Sheldrick, 2008). Experimental SAD phasing, phase improvement and initial model building were performed using the program *SOLVE*/*RESOLVE* (Terwilliger & Berendzen, 1999; Terwilliger, 2000). Approximately 50% complete main-chain models were automatically built with *RESOLVE* and were subsequently improved using *Coot* (Emsley & Cowtan, 2004). The structures of the other crystal forms were determined by molecular replacement with the program *Phaser* (McCoy *et al.*, 2007) using the α/β-domain structure of BthNK as a search probe. The cumulative intensity distribution of the AMP–Mg^{2+}–AMP complex data indicated that the crystals were twinned (Yeates, 1997). The correct molecular-replacement solutions were obtained by reduction of the space-group symmetry from $P3_121$ to $P3_1$. Using the Padilla–Yeates Twinning Server (Padilla & Yeates, 2003), the twinning operator was determined to be $(-h, h + k, -l)$ with a high twinning fraction. The twinning operator was applied in the model-refinement stage together with an estimation of the twinning fraction. All X-ray models in this study were refined with the program *REFMAC*5 (Murshudov *et al.*, 2011). The stereochemical quality of the final refined models (Table 1) was assessed using *PROCHECK* (Laskowski *et al.*, 1993). Molecular drawings were prepared using the program *PyMOL* (DeLano, 2002). Movies were created with *PyMOL*, using the atomic coordinates of ligand-free, INO-bound and MRZ–ADP-bound structures of BthNK and of additional intermediate structures generated using *LSQMAN* from the Uppsala Software Factory (Kleywegt, 1999). The relative domain rotations were analyzed using the program *DynDom* (Hayward & Berendsen, 1998). Amino-acid sequence alignment was performed using *ClustalW* (Thompson *et al.*, 1994).

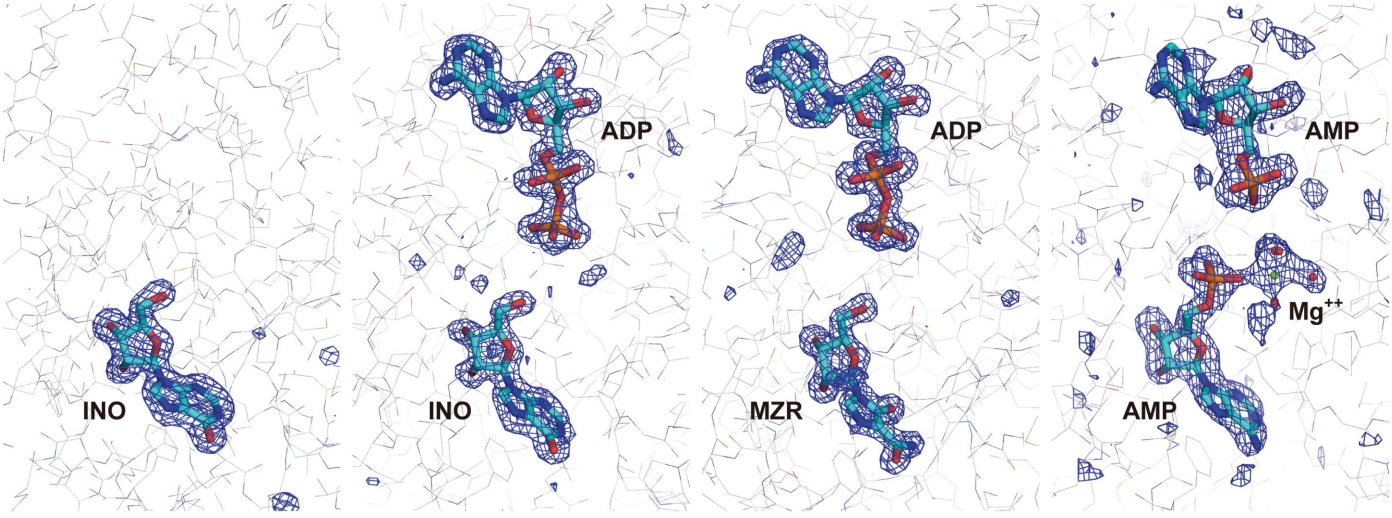

Figure 2
$F_o - F_c$ OMIT maps for the bound ligands INO (*a*), ADP–INO (*b*), ADP–MZR (*c*) and AMP–Mg^{2+}–AMP and Mg^{2+}-coordinated waters (*d*). The maps for ADP–INO, ADP–MZR and INO were contoured at the 3.0σ level and that for AMP–Mg^{2+}–AMP was contoured at the 2.0σ level. All figures are drawn in the same orientation.

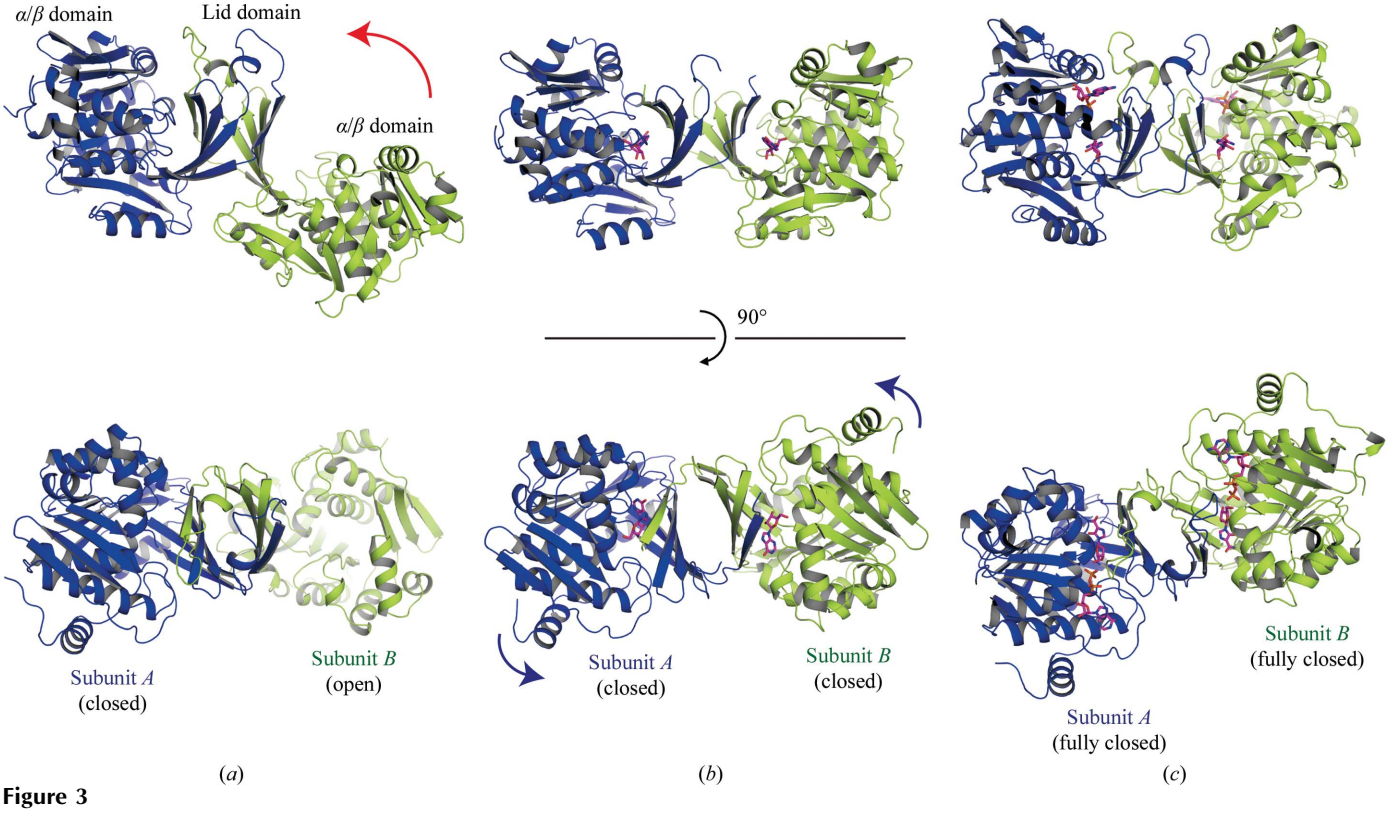

Figure 3
Dimer structures of BthNK in three distinct conformational states: BthNK in the ligand-free form (*a*), the BthNK–INO binary complex (*b*) and the BthNK–MZR–ADP ternary complex (*c*). The conformations of each subunit are labelled. The orientation of each molecule is presented by superimposing the lid domains. Arrows in red and in blue represent the orientation of domain motions from the open to the closed states and from the closed to the fully closed states, respectively. It should be noted that the relative orientations of the two-step domain motion are quite different (see also Supplementary Movies 1 and 2).

2.5. Enzyme assay

Enzyme-activity measurements for wild-type BthNK and the G170Q mutant were performed using INO, ADO and MZR as substrates. The catalytic reaction was initiated by adding the enzyme to the reaction mixture containing 30 m*M* potassium phosphate pH 7.0, 2.0 m*M* ATP, 2.0 m*M* substrate (ADO, INO or MZR) and 4.0 m*M* $MgCl_2$ and the mixture was incubated at 310 K for 10 min. Enzyme concentrations were adjusted within the linear range of the assay. The reaction was stopped by ultrafiltration (Millipore Ultrafree-MC filter unit). Reaction products (IMP, AMP or MZR-P) were detected by HPLC analysis with an Asahipak GS-320HQ column (Shodex,

Tokyo, Japan). Isocratic elution was performed using 200 m*M* sodium phosphate pH 3.0 at a flow rate of 0.5 ml min^{-1} and the elution peaks were monitored at 260 nm. The phosphorylation velocity towards each substrate of the enzyme was calculated from the reaction-product area using triplicate experiments.

3. Results and discussion

3.1. Overall structure description

BthNK is composed of 312 amino-acid residues and its three-dimensional structure is divided into two domains (Fig. 1). The larger α/β domain (residues 1–8, 49–99 and 122–312) consists of a central β-sheet formed by nine β-strands ($\beta1$, $\beta5$–$\beta6$ and $\beta9$–$\beta14$) surrounded by nine α-helices ($\alpha1$–$\alpha9$) and two 3_{10}-helices that create a common nucleoside-binding motif known as a Rossmann fold. The smaller domain, named the 'lid domain' (residues 9–48 and 100–121), is formed by five β-strands ($\beta2$–$\beta4$ and $\beta7$–$\beta8$) and one 3_{10}-helix that protrudes from the α/β domain. The lid domain is primarily responsible for dimerization *via* a number of hydrogen bonds between the main-chain carbonyl O atoms and amino N atoms of the β-strands and additional hydrophobic interactions at the core of the assembly of lid domains. The ATP- and nucleoside-binding sites are located in the deep cleft between the α/β domain and the lid domain, which has a length of about 25 Å.

3.2. Structure determination of five different crystal forms

Five crystal structures of BthNK in the ligand-free form and in various ligand complexes were determined (Table 1). In all crystal forms BthNK exhibited the common homodimeric structure of Pfk-B family enzymes as previously reported (Reddy *et al.*, 2007; Arnfors *et al.*, 2006; Sigrell *et al.*, 1998, 1999; Miallau *et al.*, 2007; Zhang *et al.*, 2004; Chua *et al.*, 2010). Gel-filtration chromatography also suggested that BthNK forms a dimer in solution (Ota, Sakasegawa *et al.*, 2008). The electron density for bound ligands is unambiguous (Fig. 2) and all ligand models (ADP, INO, MZR, AMP and AMP–Mg^{2+}) were reasonably refined with full occupancy and with low *B*-factor values (less than 20 Å^2; Table 1).

Ligand-free BthNK was crystallized in space group $P4_12_12$ and its structure was determined to 2.1 Å resolution. One dimer was observed in the asymmetric unit of the crystal and the two subunits displayed different conformations (open and closed conformations). The structure of the INO–BthNK binary complex was determined in a triclinic space group to a resolution of 1.7 Å. The unit cell was found to contain three dimers all adopting a closed conformation. In the other three crystal forms BthNK was in a fully closed conformation. These fully closed structures in different space groups superimposed well, with a root-mean-square deviation (r.m.s.d.) of less than 0.5 Å for the main-chain C^α atoms. The INO–ADP–BthNK ternary complex was crystallized in space group $P2_12_12$ and one subunit of the dimer was observed in the asymmetric unit; the structure was determined to a resolution of 1.7 Å. The other subunit of the homodimer was generated by crystallographic twofold symmetry along the *c* axis of the orthorhombic lattice. Crystals of the MZR–ADP–BthNK ternary complex were obtained under the same crystallization conditions as for the INO–ADP–BthNK complex but belonged to a different space group: $C222_1$. The structure was determined to a resolution of 1.55 Å and the asymmetric unit was found to contain one fully closed dimer. The AMP–Mg^{2+}–AMP–BthNK quaternary complex was crystallized in space group $P3_1$ in the presence of only ADP and $MgCl_2$ and the structure was determined to 2.0 Å resolution. Although the crystals of the quaternary complex were merohedrally twinned, the model was satisfactorily refined to an R_{work} and R_{free} of 0.167 and 0.204, respectively, with twinning operator $(-h, h + k, -l)$ and a twinning fraction of 0.499. Three fully closed dimers were present in the asymmetric unit. Clear electron density revealed AMP–Mg^{2+} in the nucleoside-binding pocket and AMP in the ATP-binding pocket (Fig. 2). AMP is likely to be a product of the degradation of ADP in the crystallization droplet owing to prolonged storage in the presence of Mg^{2+}. The AMP–Mg^{2+}–AMP complex was found to resemble the structure of the BthNK complex produced by phosphoryl transfer from ATP to ADO as described below.

3.3. Three distinct conformational states and comparison to related homologues

The subunit structures of BthNK show three distinct conformations: open, closed and fully closed. The orientation of the relative domain motions between the open and closed forms and between the closed and fully closed forms are quite different (Figs. 1 and 3 and Supplementary Movies 1 and 2[1]).

Ligand-free BthNK forms an asymmetric dimer composed of two identical subunits that show remarkably different conformations. Subunit *B* has an open conformation with the active-site cleft freely accessible to the solvent, while subunit *A* is rather closed and is almost identical to the closed conformation of the INO-bound binary complex. A few hydrogen bonds are formed between the lid domain and the α/β domain of subunit *A*. The main-chain O atom of Asn34(*B*) in the lid domain is hydrogen bonded to the side chain of Gln169(*A*), which is derived from the α/β domain. In addition, the side chains of Gln113(*A*) of the lid domain and Thr249(*A*) of the α/β domain form a hydrogen bond. The two subunits are unable to simultaneously adopt the open conformation because of steric hindrance between their α/β domains. Therefore, the current asymmetric dimer is likely to be one of the possible conformational states of BthNK under ligand-free conditions and the crystal lattice forces may stabilize this conformation.

The INO-bound binary-complex structure showed the closed conformation, which is similar to that of subunit *A* of the ligand-free structure, with an r.m.s.d. of about 0.3 Å. INO fits into the nucleoside-binding pocket, while the ATP-binding pocket is vacant. No electron density was observed for amino-

[1] Supplementary material has been deposited in the IUCr electronic archive (Reference: GX5193). Services for accessing this material are described at the back of the journal.

acid residues 22–33, which form a long loop in the lid domain and include a His31 for ADP binding that was observed in the ternary-complex structure. In the ligand-free structure the loop is visible in the electron-density map because the region is accidentally involved in intermolecular contacts in the crystal. The relative rotation angles of the lid domain towards the α/β domain reveal that the closed structure of BthNK is highly similar to the closed structures of MtADK (Reddy *et al.*, 2007), MjNK (Arnfors *et al.*, 2006) and *Staphylococcus aureus* LacC (Miallau *et al.*, 2007) (Table 2). Pairwise structure comparison using the *DALI* server (Holm & Park, 2000) showed that the closed BthNK (ligand-free, chain *A*) and the closed ADO binary complex of MtADK (PDB entry 2pkm, chain *A*) superimpose with an r.m.s.d. value of 2.1 Å for 312 C^{α} atoms (*Z* score 42.6).

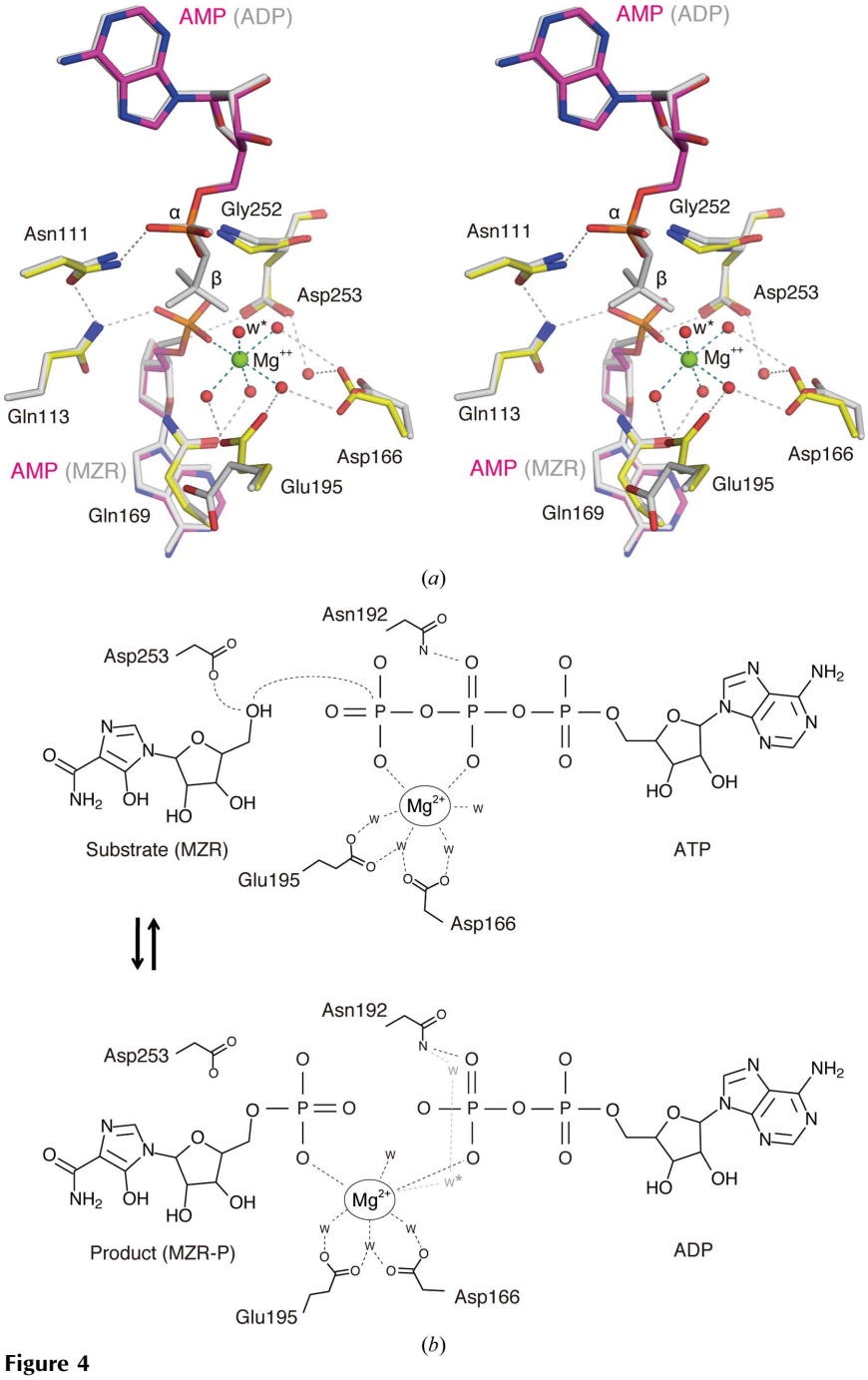

Figure 4
Catalytic mechanism of BthNK. (*a*) Stereoview superimposition of the active-site structures of the AMP–Mg^{2+}–AMP and ADP–MZR complexes. The structure of the ADP–MZR complex is shown in light grey. The Mg^{2+}-coordinated solvent molecule lying very close to the β-phosphate O atom is labelled w* (see text). (*b*) Proposed catalytic mechanism of BthNK based on the structure superimposition shown in (*a*). The w* molecules and the hydrogen bonds to the side chain of Asn192 observed in the structure of the AMP–Mg^{2+}–AMP complex are also shown in grey. Mg^{2+} is expected to maintain binding to the transferring phosphate, enabling neutralization of the negative charge throughout the reaction.

The structures of BthNK in complex with INO–ADP, MZR–ADP and AMP–Mg^{2+}–AMP show a fully closed conformation. The lid domain is closer to the α/β domain and shuts the ATP-binding pocket through interactions between the α-phosphate O atom of bound ADP and the side chains of Asn111 and His31′ (where the prime indicates a residue derived from a neighbouring subunit). These interactions may play a role in stabilizing the fully closed conformation. In MtADK the His residue is conserved, while Asn is substituted by Met (Met110) and Gln112 might play a similar role to that of Asn111 of BthNK (Supplementary Fig. 1). However, the structure of MtADK in complex with AMP-PCP (an ATP analogue) shows an open conformation and His31 and Gln112 lie far from the α-phosphate O atom of AMP-PCP, at distances of about 18 and 35 Å, respectively. In the closed structure of the ADO complex of MtADK, His31 and Gln112 are still located outside the ATP-binding pocket. It is unclear whether MtADK utilizes these residues for ATP binding.

Three distinct conformational states (open, semiclosed and closed states) have been reported in the structure analysis of *S. aureus* LacC (Miallau *et al.*, 2007). However, the semiclosed structure of LacC is a binary complex with ADP (at the ATP-binding site) and is present in a more open conformation than the closed state of BthNK (Table 2). No interactions between ADP and the lid domain were detected in the semiclosed LacC form and it is unclear whether the semiclosed structure is functionally important for LacC. Other Pfk-B dimeric structures usually adopt either an open conformation (ligand-free and ATP analogue-bound) or a closed conformation (substrate-bound). The ADO complex of MtADK is in a closed conformation, while the AMP-PCP complex shows an open conformation similar to its ligand-free form (Reddy *et al.*, 2007). Ribose-bound EcRK

also showed a closed conformation similar to that of the ternary complex with AMP-PNP and ribose, while ligand-free EcRK showed an open form (Sigrell *et al.*, 1999). These observations suggest that the conformational change from an open to a closed form is induced by substrate binding rather than by ATP or its analogues. In contrast, BthNK forms a closed conformation in both the ligand-free and the INO-bound forms. These results suggest that BthNK might exist in a conformational equilibrium between open and closed forms under ligand-free conditions. Once the substrate nucleoside is bound to the closed BthNK, the subsequent induced-fit recognition of ATP could stabilize the fully closed conformation that promotes the phosphoryl-transfer reaction.

Table 2
Relative domain rotations of BthNK and related homologues.

Chain *X*	Chain *Y*	Relative rotation† (°)
Comparison within BthNK structures		
Ligand-free BthNK chain *A* (closed)	Ligand-free BthNK chain *B* (open)	−56.9
	BthNK–INO chain *A* (closed)	ND‡
	BthNK–INO–ADP chain *A* (fully closed)	23.3
	BthNK–MZR–ADP chain *A* (fully closed)	25.2
	BthNK–AMP–Mg–AMP chain *A* (fully closed)	26.4
Comparison of closed BthNK in ligand-free form and MtADK/MjNK/LacC in various conformations		
Ligand-free BthNK chain *A* (closed)	MtADK (PDB entry 2pkf, chain *A*; open)	−38.9
	MtADK (PDB entry 2pkm, chain *A*; closed)	ND‡
	MjNK (PDB entry 2c49, chain *B*; open)	−20§
	MjNK (PDB entry 2c49, chain *A*; closed)	0§
	LacC (PDB entry 2jgv, chain *A*; open)	−32§
	LacC (PDB entry 2jgv, chain *D*; semiclosed)	−18§
	LacC (PDB entry 2jg1, chain *C*; closed)	0§

† Negative values indicate that chain *X* is in a more closed conformation than chain *Y*, and *vice versa*. ‡ ND indicates that domain rotations were not detected according to the *DynDom* criteria (Hayward & Berendsen, 1998). § The program *DynDom* (Hayward & Berendsen, 1998) did not work owing to low sequence identity between BthNK and MjNK/LacC. Thus, the relative rotation angles were roughly estimated using *Coot* (Emsley & Cowtan, 2004).

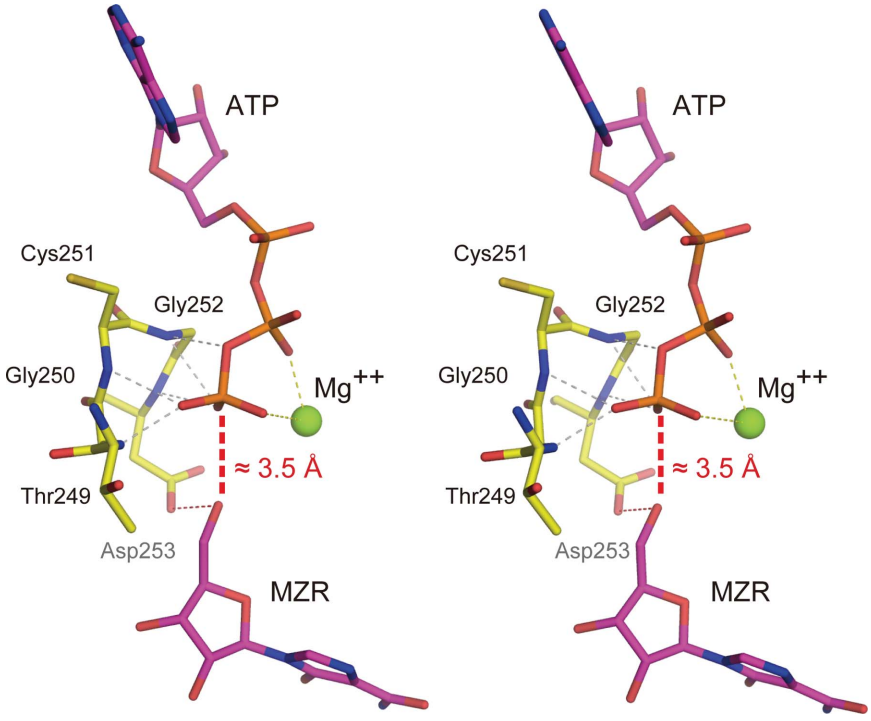

Figure 5
Stereoview showing the putative Michaelis complex of BthNK. This model is based on the structure of the ADP–MZR complex. The γ-phosphate of ATP was modelled into the active site based on the position of the bound ADP. Mg^{2+} is modelled by superimposing the structure of the AMP–Mg^{2+}–AMP complex on that of the ADP–MZR complex. The interatomic interactions shown as dashed lines are within distances of 2.4–3.2 Å. In this model, the distance between the γ-phosphorus (P^{γ}) of ATP and the O atom of the 5′-hydroxyl (nucleophile) of MZR is approximately 3.5 Å, with an O3β—$P^{\gamma}\cdots$O angle (nucleophile) that is almost linear (171°).

3.4. Proposed catalytic mechanism based on fully closed structures

BthNK requires a divalent cation such as Mg^{2+} for catalytic reaction (Ota, Sakasegawa *et al.*, 2008). Attempts to solve the crystal structure of BthNK in complex with an ATP analogue in the presence and absence of Mg^{2+} were not successful. However, in the present study the structure of BthNK with AMP bound at the ATP-binding site and AMP–Mg^{2+} bound at the nucleoside-binding site was successfully determined. The bound Mg^{2+} was probably detected owing to a high concentration of $MgCl_2$ in the crystallization solution. Mg^{2+} exhibited an octahedral coordination with the 5′-phosphate O atom of AMP and five additional solvent molecules. Four of the five solvent molecules interacted with the side chains of Asp166, Glu195 and Gln169, with distances of 2.6–2.8 Å, and the remaining solvent molecule (w*) interacted indirectly with Asn192 *via* an additional solvent molecule (Fig. 4*b*). Asn192 and Glu195 correspond to the N and E of the N*XX*E motif, which is an important sequence for Mg^{2+} binding in the Pfk-B family (Supplementary Fig. 1; Maj *et al.*, 2002). Superposition of the AMP–Mg^{2+}–AMP and ADP–MZR (or ADP–INO) complex structures allowed us to build a putative AMP–Mg^{2+}–ADP complex model (Fig. 4). In this model, one of the β-phosphate O atoms of ADP lies very close to w* at a distance of about 1.0 Å and is separated from the Mg^{2+} by approximately 2.8 Å. The model allows the possible coordination of the β-phosphate O atom to Mg^{2+} in place of w*. Considering these binding conditions, the bound Mg^{2+} would not be a crystallization artifact but would instead be functionally important.

Accordingly, a possible mechanism for the phosphoryl-transfer reaction of

BthNK has been proposed (Fig. 4*b*). Initially, the substrate nucleoside and ATP are bound to the binding sites of BthNK. Mg^{2+} is also in contact with the γ- and β-phosphate O atoms, together with the coordination of presumably four solvent molecules that are stabilized by the side chains of Asp166, Gln169 and Glu195 and nearby solvent molecules, as observed in the structure of the AMP–Mg^{2+}–AMP complex. After proton abstraction from the 5′-hydroxyl of the nucleoside ribose by Asp253 to generate a nucleophile, the S_N2 reaction occurs by nucleophilic attack on the γ-phosphorus of ATP. In previous structural studies on EcRK and MtADK, the distances between the γ-phosphate and ribose 5′-hydroxyl are greater than the optimal distance for nucleophilic attack, thus suggesting that further conformational change to a more closed form or water-mediated reaction could occur (Reddy *et al.*, 2007; Sigrell *et al.*, 1999). In contrast, the current fully closed structures of BthNK indicate that the modelled γ-phosphate is precisely located at the 'anion hole' formed by the main-chain N atoms of residues 250–253 and the distance between the nucleophile O atom and the modelled γ-phosphorus is about 3.5 Å, with a nearly linear (about 171°) O3β—P$^{\gamma}\cdots$O (nucleophile) angle. These values are compatible with direct nucleophilic attack to produce a phosphorylated nucleoside *via* a pentacoordinate intermediate, implying that the current fully closed conformation would nearly resemble that of the assumed transient Michaelis complex (Fig. 5). This phosphoryl-transfer mechanism is similar to that proposed in structural studies on human ADK (Mathews *et al.*, 1998) and *S. aureus* LacC (Miallau *et al.*, 2007). Interestingly, the present results show that the Mg^{2+} is in direct contact with the 5′-phosphate of the product AMP. Mg^{2+} might remain in contact with the two phosphate O atoms while being stabilized by the solvent-mediated side chains of Asp166 and Glu195, thus maintaining neutralization of the negative charge on the transferring phosphate throughout the reaction.

3.5. Insights into nucleoside binding and selectivity

BthNK exhibits phosphoryl-transfer activity towards various nucleosides, in particular INO, ADO and MZR. The current structures reveal that the solvent molecules form hydrogen bonds to the N atoms of the base moieties of INO or AMP. The carboxamide group of MZR also forms hydrogen bonds to the solvent molecules (Fig. 6). Considering the exposure of the base moiety to the solvent in the closed conformation, it is indeed impossible to discriminate between the slight differences in atomic composition of adenine and hypoxanthine. In contrast, MtADK is highly specific for ADO and its activity towards various other nucleosides, including INO, was below the detection limit (Long *et al.*, 2003). The MtADK structure with bound ADO clearly showed that the side chain of Gln170 forms double hydrogen bonds to the two N atoms of the adenine base (Fig. 7). The Gln173 residue of MtADK corresponds to Gly170 in BthNK and accordingly the solvent is accessible to the base moiety of the bound nucleoside. Whether this glutamine residue is actually responsible for the ADO specificity remains unclear. To test whether Gly170 is really responsible for the promiscuity of BthNK, we generated the G170Q mutant of BthNK and performed an enzyme assay using INO, ADO and MZR as substrates. The reaction products IMP, AMP and MZR-P were directly detected by HPLC analysis, which enabled a more accurate assessment than that of the previous assay method by coupling multiple enzyme reaction systems (Ota, Sakasegawa *et al.*, 2008). The results demonstrated that the G170Q mutation significantly decreases the activity towards INO and MZR and slightly increases the activity towards ADO (Table 3), clearly indicating that the glutamine is a key determinant of ADO specificity in the G170Q mutant of BthNK. In MtADK, the side-chain N atom of Gln173 forms hydrogen bonds to N1 of ADO and the main-chain carbonyl O atom of Asn47, while the side-chain O atom of Gln173 is hydrogen bonded to N6 of ADO. In the model of INO/MZR binding, steric hindrance between H atoms or electrostatic repulsion between carbonyl O atoms could not be avoided (Fig. 8). This incompatibility is likely to decrease the binding affinity of INO/MZR.

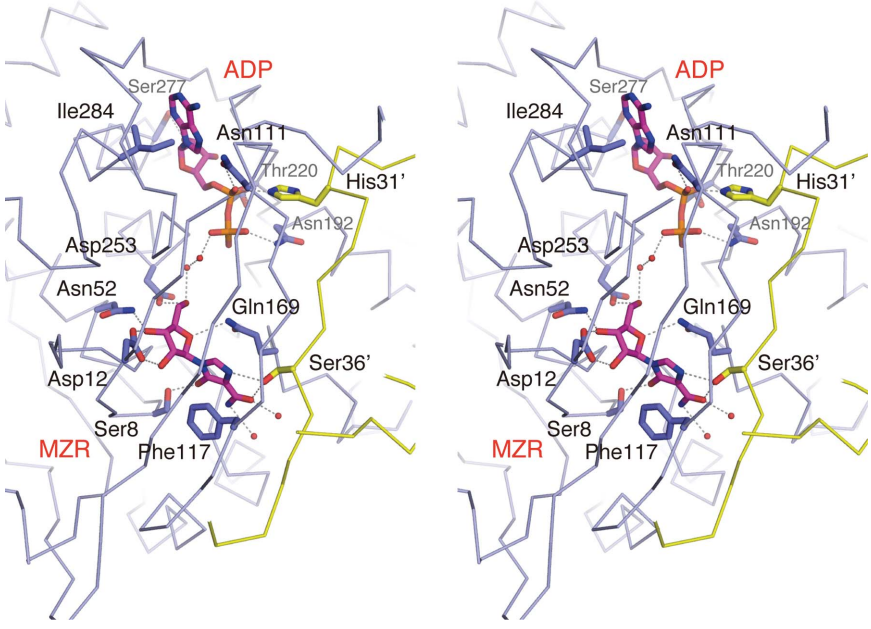

Figure 6
Stereoview C$^{\alpha}$ trace of the active-site structure of BthNK. The side chains of the substrate-binding residues and the bound MZR/ADP are depicted as sticks. The solvent atoms are shown in red. Possible hydrogen bonds are indicated as dashed lines. For the MZR and ADP molecules, C atoms are coloured magenta, O atoms red, N atoms blue and P atoms orange. The protein backbone is coloured light blue. The backbone of the neighbouring subunit is shown in yellow.

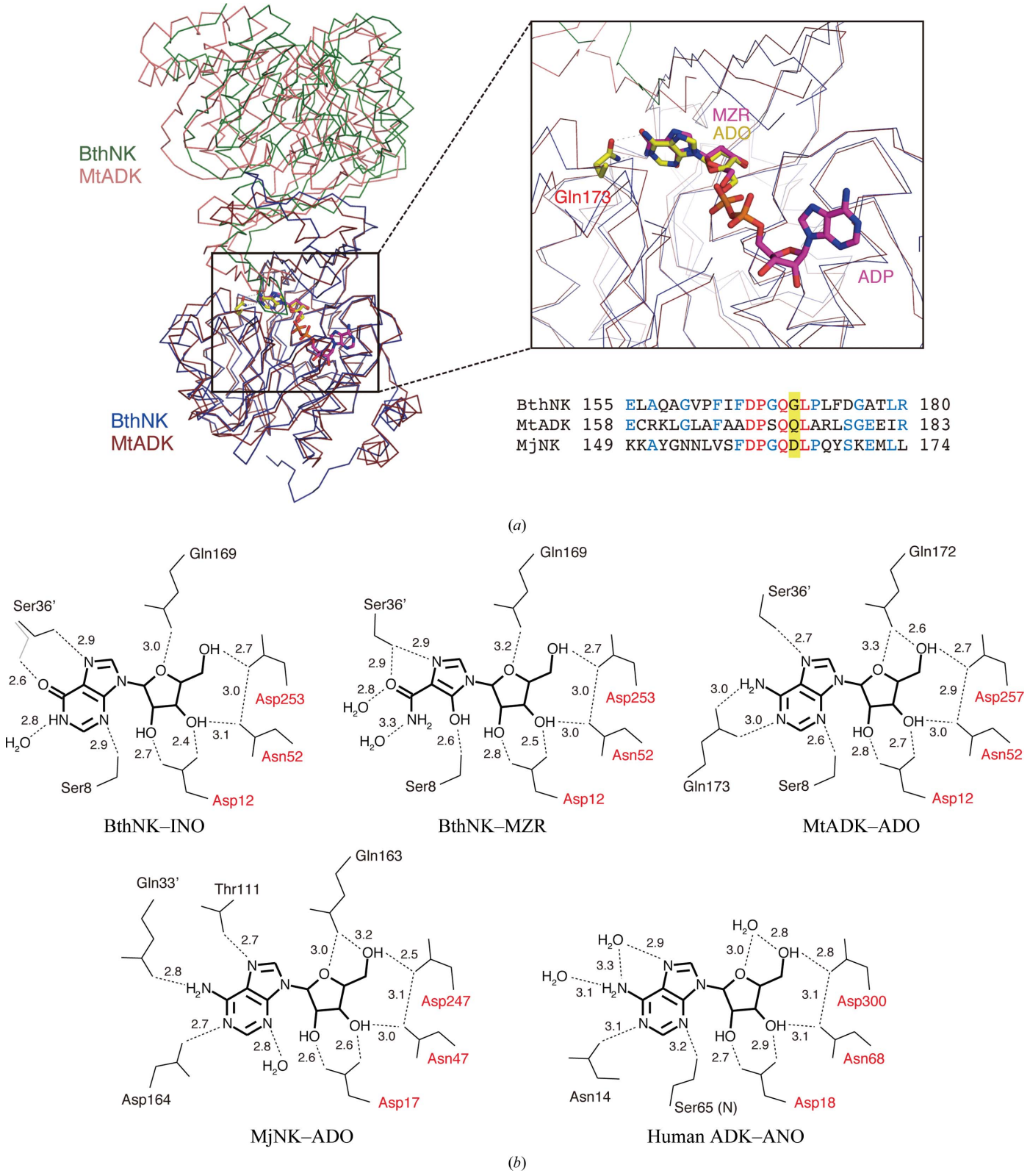

Figure 7
Comparison of nucleoside-binding sites between BthNK, MtADK and related enzymes. (*a*) Superimposition of BthNK and MtADK dimers and close-up view of the nucleoside-binding site. The superimposition was performed using only the α/β domains of the lower subunit, showing that the conformation of BthNK is more closed than that of MtADK. The bound ADP, MZR and ADO and the side chain of Gln170 of MtADK are depicted in stick representation. Sequence alignment for the region including Gln170 is also shown. Full sequence alignment is shown in Supplementary Fig. 1. (*b*) Comparison of the hydrogen-bonding pattern at the nucleoside-binding site between BthNK, MtADK (Reddy *et al.*, 2007), MjNK (Arnfors *et al.*, 2006) and human ADK (Mathews *et al.*, 1998). Possible hydrogen bonds (distances of 3.3 Å or below) are shown as dashed lines. Primes indicate residues from the neighbouring subunit. The conserved residues for ribose binding (two Asp and one Asn residues) are shown in red.

Mammalian ADK is known to exhibit broad nucleoside specificity (Miller *et al.*, 1979). The structure of human ADK with bound ADO revealed that two water molecules form hydrogen bonds to N7 and N6 of the adenine base (Fig. 7*b*; Mathews *et al.*, 1998). This may account for its tolerance toward the base moiety of the nucleoside. MjNK also exhibits broad nucleoside specificity and particularly high activity towards INO, guanosine and cytidine (Hansen *et al.*, 2007). However, the structure of MjNK revealed that the bound ADO is buried inside the polypeptide chain and elaborate interatomic interactions exist. The side chain of Asp164, which corresponds to the Gly170 residue of BthNK, interacts with N1 of ADO and the side chain of His13. The side chain of Gln33′ forms double hydrogen bonds to N6 of ADO and the main-chain carbonyl of Gln163. This glutamine residue is not present in BthNK, human ADK or other homologues (Supplementary Fig. 1). Thr111 also forms hydrogen bonds to N7 of ADO in place of Ser36′ of BthNK/MtADK. Additionally, one solvent molecule forms a hydrogen bond to N3 of ADO in MjNK owing to the absence of the amino-acid residue corresponding to Ser8 of BthNK/MtADK (Fig. 7*b*). The different environment of the base-binding pocket of MjNK suggests the presence of a different base-recognition mechanism presumably enabling binding of INO, guanosine and cytidine. These observations indicate that the basic recognition mechanism of nucleoside/ADO kinases is highly diversified and might have been independently acquired during molecular evolution.

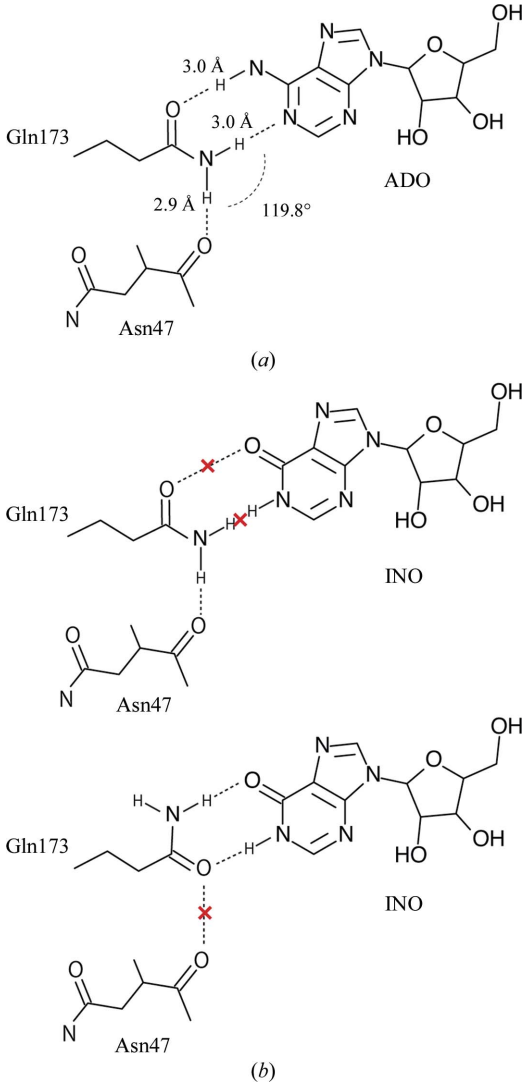

Figure 8
Possible mechanism of adenine base specificity by a glutamine residue. (*a*) The ADO-binding site is observed in the MtADK structure (PDB entry 2pkm). The side chain of Gln173 forms triple hydrogen bonds to the two N atoms of adenine and the main-chain carbonyl O atom of Asn47. (*b*) The expected INO-binding site is in the same position as that for ADO. Steric hindrance between H atoms or electrostatic repulsion between carbonyl O atoms is likely to preclude the binding of INO to MtADK. The substitution of Gln for Gly allows BthNK to have binding affinity towards ADO, INO and MZR.

Table 3
Specific activities of wild-type BthNK and the G170Q mutant.

Values in parentheses refer to the relative activity compared with the specific activity of wild-type BthNK.

Enzyme	Wild type		G170Q mutant	
Substrate	Specific activity (μmol min^{-1} mg^{-1})	Relative activity (%)	Specific activity (μmol min^{-1} mg^{-1})	Relative activity (%)
INO	3.57 ± 0.53	68.1	0.41 ± 0.14	6.9 (11.5)
ADO	5.24 ± 0.35	100.0	5.91 ± 1.16	100.0 (112.8)
MZR	2.49 ± 0.20	47.5	0.10 ± 0.10	1.7 (4.0)

4. Conclusions

In summary, we have determined structures of BthNK in the ligand-free form and in complex with INO, ADP–INO, ADP–MZR and AMP–Mg^{2+}–AMP. The structures revealed that the BthNK monomer is found in three distinct conformations, namely open, closed and fully closed forms, in response to ligand binding. The fully closed structure resembles the conformation of the transient state during the phosphoryl-transfer reaction and suggests a possible mechanism for the Mg^{2+}-dependent catalytic reaction. Unlike the closed crystal structures observed for MtADK complexes, the fully closed structures of the BthNK ternary and quaternary complexes observed here suggest that, as also observed for human ADK and *S. aureus* LacC, phosphoryl transfer occurs *via* an in-line direct nucleophilic attack mechanism. Moreover, we identified the key residue (Gly170) that confers broad substrate specificity to BthNK by exposing the base moiety of the bound nucleoside to the solvent. In addition, the G170Q mutation was confirmed to significantly increase ADO specificity. These results significantly contribute to our understanding of the catalytic and nucleoside-binding mechanisms of BthNK and related enzymes of the Pfk-B family.

We thank the technical staff at Photon Factory (PF) for their kind support during the X-ray diffraction studies. Synchrotron-radiation experiments were conducted under the approval of PF (2009G517).

References

Abe, Y., Tsuji, Y., Hisano, M., Nakada, M., Miura, K., Watanabe, S., Odajima, Y. & Iikura, Y. (2004). *Pediatr. Int.* **46**, 597–600.

Arnfors, L., Hansen, T., Schönheit, P., Ladenstein, R. & Meining, W. (2006). *Acta Cryst.* D**62**, 1085–1097.

Battye, T. G. G., Kontogiannis, L., Johnson, O., Powell, H. R. & Leslie, A. G. W. (2011). *Acta Cryst.* D**67**, 271–281.

Cabrera, R., Babul, J. & Guixé, V. (2010). *Arch. Biochem. Biophys.* **502**, 23–30.

Chua, T. K., Seetharaman, J., Kasprzak, J. M., Ng, C., Patel, B. K., Love, C., Bujnicki, J. M. & Sivaraman, J. (2010). *J. Struct. Biol.* **171**, 397–401.

Dauter, Z., Dauter, M. & Rajashankar, K. R. (2000). *Acta Cryst.* D**56**, 232–237.

DeLano, W. L. (2002). *PyMOL*. http://www.pymol.org.

Emsley, P. & Cowtan, K. (2004). *Acta Cryst.* D**60**, 2126–2132.

Hansen, T., Arnfors, L., Ladenstein, R. & Schönheit, P. (2007). *Extremophiles*, **11**, 105–114.

Hayward, S. & Berendsen, H. J. (1998). *Proteins*, **30**, 144–154.

Heinig, M. & Frishman, D. (2004). *Nucleic Acids Res.* **32**, W500–W502.

Hemsley, A., Arnheim, N., Toney, M. D., Cortopassi, G. & Galas, D. J. (1989). *Nucleic Acids Res.* **17**, 6545–6551.

Hiramitsu, T., Ota, H., Watarai, Y., Achiha, M., Fukami, H., Sakasegawa, S., Hino, E., Yamaguchi, T., Ueda, S., Kagimoto, Y., Tamura, T. & Uchida, K. (2011). *J. Biosci. Bioeng.* **112**, 205–207.

Holm, L. & Park, J. (2000). *Bioinformatics*, **16**, 566–567.

Kleywegt, G. J. (1999). *Acta Cryst.* D**55**, 1878–1884.

Koyama, H. & Tsuji, M. (1983). *Biochem. Pharmacol.* **32**, 3547–3553.

Kusumi, T., Tsuda, M., Katsunuma, T. & Yamamura, M. (1989). *Cell Biochem. Funct.* **7**, 201–204.

Laskowski, R. A., MacArthur, M. W., Moss, D. S. & Thornton, J. M. (1993). *J. Appl. Cryst.* **26**, 283–291.

Long, M. C., Escuyer, V. & Parker, W. B. (2003). *J. Bacteriol.* **185**, 6548–6555.

Maj, M. C., Singh, B. & Gupta, R. S. (2002). *Biochemistry*, **41**, 4059–4069.

Mathews, I. I., Erion, M. D. & Ealick, S. E. (1998). *Biochemistry*, **37**, 15607–15620.

McCoy, A. J., Grosse-Kunstleve, R. W., Adams, P. D., Winn, M. D., Storoni, L. C. & Read, R. J. (2007). *J. Appl. Cryst.* **40**, 658–674.

Miallau, L., Hunter, W. N., McSweeney, S. M. & Leonard, G. A. (2007). *J. Biol. Chem.* **282**, 19948–19957.

Miller, R. L., Adamczyk, D. L., Miller, W. H., Koszalka, G. W., Rideout, J. L., Beacham, L. M. III., Chao, E. Y., Haggerty, J. J., Krenitsky, T. A. & Elion, G. B. (1979). *J. Biol. Chem.* **254**, 2346–2352.

Mitani, Y., Meng, X., Kamagata, Y. & Tamura, T. (2005). *J. Bacteriol.* **187**, 2582–2591.

Mizuno, K., Tsujino, M., Takada, M., Hayashi, M. & Atsumi, K. (1974). *J. Antibiot.* **27**, 775–782.

Murshudov, G. N., Skubák, P., Lebedev, A. A., Pannu, N. S., Steiner, R. A., Nicholls, R. A., Winn, M. D., Long, F. & Vagin, A. A. (2011). *Acta Cryst.* D**67**, 355–367.

Nakashima, N. & Tamura, T. (2004). *Biotechnol. Bioeng.* **86**, 136–148.

Ota, H., Sakasegawa, S., Yasuda, Y., Imamura, S. & Tamura, T. (2008). *FEBS J.* **275**, 5865–5872.

Ota, H., Yasuda, Y., Sakasegawa, S., Imamura, S. & Tamura, T. (2008). *J. Biosci. Bioeng.* **106**, 511–514.

Otwinowski, Z. & Minor, W. (1997). *Methods Enzymol.* **276**, 307–326.

Padilla, J. E. & Yeates, T. O. (2003). *Acta Cryst.* D**59**, 1124–1130.

Reddy, M. C., Palaninathan, S. K., Shetty, N. D., Owen, J. L., Watson, M. D. & Sacchettini, J. C. (2007). *J. Biol. Chem.* **282**, 27334–27342.

Sheldrick, G. M. (2008). *Acta Cryst.* A**64**, 112–122.

Sigrell, J. A., Cameron, A. D., Jones, T. A. & Mowbray, S. L. (1998). *Structure*, **6**, 183–193.

Sigrell, J. A., Cameron, A. D. & Mowbray, S. L. (1999). *J. Mol. Biol.* **290**, 1009–1018.

Stypinski, D., Obaidi, M., Combs, M., Weber, M., Stewart, A. J. & Ishikawa, H. (2007). *Br. J. Clin. Pharmacol.* **63**, 459–468.

Terwilliger, T. C. (2000). *Acta Cryst.* D**56**, 965–972.

Terwilliger, T. C. & Berendzen, J. (1999). *Acta Cryst.* D**55**, 849–861.

Thompson, J. D., Higgins, D. G. & Gibson, T. J. (1994). *Nucleic Acids Res.* **22**, 4673–4680.

Winn, M. D. *et al.* (2011). *Acta Cryst.* D**67**, 235–242.

Wu, L.-F., Reizer, A., Reizer, J., Cai, B., Tomich, J. M. & Saier, M. H. (1991). *J. Bacteriol.* **173**, 3117–3127.

Yeates, T. O. (1997). *Methods Enzymol.* **276**, 344–358.

Yokota, S. (2002). *Pediatr. Int.* **44**, 196–198.

Zhang, Y., Dougherty, M., Downs, D. M. & Ealick, S. E. (2004). *Structure*, **12**, 1809–1821.